Wang J, Pielak R M, McClintock M A, et al. Solution structure and functional analysis of the influenza B proton channel. Nat Struct Mol Biol, 2009

4 **AUTHORS**, INCLUDING:

Junfeng Wang
Hefei Institute of Physical Sciences, Chines…
34 PUBLICATIONS   929 CITATIONS

Rafal M Pielak
University of California, Berkeley
22 PUBLICATIONS   702 CITATIONS

James J Chou
Harvard Medical School
90 PUBLICATIONS   5,342 CITATIONS

nature
structural &
molecular biology

Solution structure and functional analysis of the influenza B proton channel

Junfeng Wang[1], Rafal M Pielak[1,2], Mark A McClintock[1] & James J Chou[1]

Influenza B virus contains an integral membrane protein, BM2, that oligomerizes in the viral membrane to form a pH-activated proton channel. Here we report the solution structures of both the membrane-embedded channel domain and the cytoplasmic domain of BM2. The channel domain assumes a left-handed coiled-coil tetramer formation with a helical packing angle of −37° to form a polar pore in the membrane for conducting ions. Mutagenesis and proton flux experiments identified residues involved in proton relay and suggest a mechanism of proton conductance. The cytoplasmic domain of BM2 also forms a coiled-coil tetramer. It has a bipolar charge distribution, in which a negatively charged region interacts specifically with the M1 matrix protein that is involved in packaging the genome in the virion. This interaction suggests BM2 also recruits matrix proteins to the cell surface during virus budding, making BM2 an unusual membrane protein with the dual roles of conducting ions and recruiting proteins to the membrane.

Influenza B virus is an important constituent of human seasonal flu that accounts for about 50% of all influenza disease in recent years (according to the US Centers for Disease Control website). The virion contains an integral membrane protein, BM2, that is essential for virus replication[1] and oligomerizes in the viral membrane to form a pH-activated proton channel[2]. The recognized role of the proton channel is to equilibrate pH both across the viral membrane during viral entry and across the trans-Golgi membrane of infected cells during viral maturation[3,4].

BM2 protein is a single-span membrane protein of 109 residues; it is a homotetramer in its native state[5]. Although BM2 and AM2 (the proton channel from influenza A) both conduct protons and influenza B is the closest relative of influenza A virus, the two proteins are different in amino acid sequence and in channel properties. Except for the HXXXW sequence motif in the transmembrane (TM) domain that is essential for pH sensing and channel gating, BM2 shares almost no sequence identity with AM2 (**Supplementary Fig. 1**). Unlike that of AM2, the BM2 proton conductance is completely insensitive to amantadine and rimantadine, which were the first effective drugs licensed for influenza treatment[6]. BM2 channel activity is also higher than that of AM2 (ref. 6). A wealth of structural information is available for the channel domain of AM2, including models derived from biochemical and spectroscopic data[7–9] as well as high-resolution NMR[10,11] and X-ray[12] structures. Cysteine scanning mutagenesis suggests a model for the channel domain of BM2 (ref. 13), but no high-resolution structures have been determined. In addition to the channel domain, BM2 and AM2 have relatively large cytoplasmic regions compared to other influenza surface proteins, for which there is no structural information. It has been suggested that the cytoplasmic regions of AM2 and BM2 are important for proper virus assembly[14–17].

We had determined the structure of the AM2 channel bound to the drug rimantadine and proposed an allosteric mechanism for drug inhibition and drug resistance[10,18]. In an effort to understand how the BM2 channel works, we determined the solution structures of the membrane-embedded channel domain and the C-terminal cytoplasmic domain of BM2. The many differences in channel assembly between BM2 and AM2 explain the properties unique to the BM2 channel, such as drug resistance and higher proton conductance. We also carried out mutagenesis and liposomal proton flux assays to identify residues involved in proton relay across the channel. The cytoplasmic domain of BM2 is also a coiled-coil tetramer, and its unusually large electrostatic dipole moment suggests a role in molecular recognition. NMR chemical shift perturbation experiments showed that the cytoplasmic domain interacts specifically with the M1 matrix protein. Thus, in addition to conducting protons, BM2 is involved in viral assembly, probably by recruiting the matrix proteins to the cell surface during virus budding.

RESULTS
Solution structure of BM2
For proteins that contain membrane-embedded and cytoplasmic domains, it is difficult to find a detergent that preserves the structural integrity of both domains. We screened the intact full-length BM2 in many detergents, but these efforts yielded no workable NMR spectra. We then established two protein constructs corresponding to two separate functional domains of BM2 and determined their NMR structures (see NMR structural statistics in **Table 1** and **Supplementary Fig. 2**). In dihexonyl phosphocholine (DHPC) micelles, $BM2_{1–33}$, a construct encompassing residues 1–33, forms a coiled-coil tetramer with a packing angle of about −37° (**Fig. 1a**). The tetramer has a well

Table 1 NMR and refinement statistics for protein structures

	Residues 2–3	Residues 44–103
NMR distance and dihedral constraints		
Distance constraints		
Total NOE	232 × 4	356 × 4
Intra-residue	57 × 4	138 × 4
Inter-residue	164 × 4	202 × 4
Sequential ($|i - j| = 1$)	96 × 4	118 × 4
Medium range ($|i - j| \leq 4$)	68 × 4	75 × 4
Long range ($|i - j| \geq 5$)	0	9 × 4
Intermolecular	11 × 4	16 × 4
Hydrogen bonds	38 × 4	84 × 4
Total dihedral angle restraints	51 × 4	131 × 4
ϕ (TALOS)	26 × 4	50 × 4
ψ (TALOS)	25 × 4	50 × 4
χ_1 (J couplings)	0	31 × 4
Total residual dipolar couplings	0	56 × 4
Backbone NH	0	56 × 4
Structure statistics		
Violations (mean ± s.d.)		
Distance constraints (Å)	0.046 ± 0.0021	0.068 ± 0.0014
Dihedral angle constraints (°)	0.247 ± 0.115	3.20 ± 0.098
Max. dihedral angle violation (°)	0.452	3.45
Max. distance constraint violation (Å)	0.049	0.070
Q (%)		0.120
Deviations from idealized geometry		
Bond lengths (Å)	0.0035 ± 0.00013	0.0029 ± 0.000049
Bond angles (°)	0.40 ± 0.023	0.42 ± 0.0068
Impropers (°)	0.27 ± 0.011	0.36 ± 0.0067
Average pairwise r.m.s. deviation[a] (Å)		
Heavy	1.06	1.38
Backbone	0.70	0.92

[a]Pairwise r.m.s. deviation was calculated among 15 refined structures.

defined hydrophilic channel that is occluded by Phe5 and Trp23 at the N- and C-terminal ends, respectively (**Fig. 1b**). The structure was determined at pH 7.5 and, thus, corresponds to the closed state. When reconstituted into liposomes made from *Escherichia coli* lipid extract, BM2$_{1–33}$ shows specific proton conductance that is completely insensitive to 50 µM of rimantadine (**Supplementary Fig. 3**). For structural study of the cytoplasmic domain, we used a construct, BM2$_{26–109}$, that includes the entire predicted extramembrane region (residues 44–109) as well as six N-terminal membrane-anchor residues that overlap with BM2$_{1–33}$. When bound to 14:0 *lyso*-phosphoglycerol (LMPG) micelles, the structured region of BM2$_{26–109}$, for which the atomic coordinates are defined by NMR restraints, commences at Pro44 and ends at Leu103 (**Fig. 1c**). Residues 45–85 form an uninterrupted helix that oligomerizes into a left-handed coiled-coil tetramer. A hairpin-like structure, consisting of residues 86–92, connects the coiled-coil structure to a short amphipathic helix that is roughly perpendicular to the coiled-coil helix. This short helix, composed of residues 93–103, packs against the hairpin region of the adjacent subunit such that the hydrophobic sides of the amphipathic helix and hairpin are protected from the solvent. Although no intersubunit nuclear Overhauser effects (NOEs) were observed for residues 34–43, the region that connects the TM and cytoplasmic domain, residues 39–45 show NOEs with respect to the glycerol protons of LMPG headgroup (**Supplementary Fig. 4**). By translating the protein-LMPG NOEs into semiquantitative distance restraints between the protein protons and an imaginary plane representing the headgroup of the lipid bilayer[19], we modeled the full-length BM2 structure using all NMR restraints measured for the TM and cytoplasmic domains. The model (**Fig. 1d**) provides a qualitative view of the overall conformation of the BM2 tetramer with respect to the lipid bilayer, although the protein-LMPG interactions observed here may not reflect those in the membrane environment.

The coiled-coil structure of the channel domain shows at least two heptad repeats: one from Leu8 at position *g* to Ile14 at position *f*, and the other from Leu15 at position *g* to Ile21 at position *f* (**Fig. 2a**). Positions *a* and *d*, which constitute the core of the coiled-coil tetramer, are occupied mostly by hydrophilic residues such as Ser9, Ser12 and Ser16. His19 at position *d* and Trp23 at position *a* are also pore-lining, consistent with their essential roles in pH sensing and channel gating. Positions *g* and *e* are occupied by Leu8 and Leu15 and Phe13 and Phe20, respectively, to allow for peripheral hydrophobic interactions that stabilize helical packing. The above amino acids in positions *a*, *d*, *g* and *e* are conserved in all sequenced BM2 variants (**Supplementary Fig. 5a**). The rest of the positions of the heptad repeat (*b*, *c* and *f*) are occupied by hydrophobic residues (with the exception of Ser11), which form the hydrophobic surface of the tetramer for membrane partition. This arrangement for coiled-coil assembly in membrane is opposite to that of water-soluble coiled-coil tetramers, in which positions *a* and *d* are typically hydrophobic residues and positions *g* and *e* are polar residues[20] (**Fig. 2a**). The structure of the BM2 TM domain thus provides an example for designing membrane-embedded coiled-coil tetramers with a hydrophilic pore, with far-reaching implications for ion channel design.
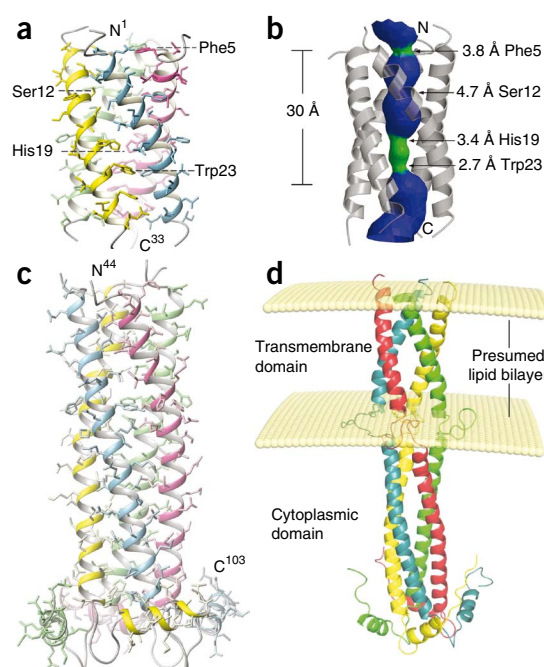
Figure 1 Solution structure of BM2 from influenza B virus. (**a**) Structure of the channel domain (residues 1–33) in DHPC micelles at pH 7.5. (**b**) The pore surface of the channel domain calculated using the program HOLE[26]. The channel is colored in green for regions wider than 2.7 Å and narrower than 4.6 Å and colored in blue for regions wider than 4.6 Å. (**c**) The structured cytoplasmic domain (residues 44–103) of BM2$_{26–109}$ anchored to LMPG micelles at pH 6.8. (**d**) A model of the full-length BM2 built with the structures of the channel and cytoplasmic domains. The positioning of the two domains and their localization relative to the lipid bilayer were modeled using intrasubunit and protein-LMPG NOEs, measured for residues 29–43 of the BM2$_{26–109}$ construct.

Figure 2 Assembly of the H^{+} conducting pore. (**a**) Comparison of helical wheel representations of coiled-coil assemblies of the BM2 channel domain (left) and GCN4 (right)[20], illustrating the concept of using the principle of coiled-coil packing to form a polar pore in a hydrophobic environment. Residues with negative or positive hydropathy index are colored in red and black, respectively. (**b**) The pore-lining residues revealed by removing one of the four TM helices. (**c**) Proton conduction traces of BM2$_{1-33}$ and its mutants. Protein concentration is the same for all BM2$_{1-33}$ variants. Rates of proton flux are reported in **Table 2**.

Polar residues mediate proton conduction

To investigate the mechanism of proton conductance, we mutated polar pore residues to alanines and quantified the effect of the single mutations on proton conductance using a liposomal proton flux assay. In this assay, we used a proton gradient to drive proton conductance because this most directly mimics what happens in the endosome after endocytosis[4]. Known quantities of BM2$_{1-33}$ variants were reconstituted into liposomes that were made with identical pH and ion concentrations inside and outside, but were strongly buffered inside and weakly buffered outside. Proton conductance was initiated under conditions of rapid solution mixing by the addition of concentrated acid to the external solution, then measured as the increase in pH of the external solution as protons moved down the pH gradient into the liposomes[18] (**Supplementary Fig. 3a**). As a validation of the assay, we verified (i) that nearly no proton translocation is observed in the absence of proton channel (**Supplementary Fig. 3b**); (ii) that the specific conductance of the wild-type (WT) BM2$_{1-33}$ is completely insensitive to rimantadine (**Supplementary Figs. 3c,d**); and (iii) that the specific conductance of the WT AM2 construct (AM2$_{18-60}$, containing residues 18 through 60) is inhibited by as little as 10 μM of rimantadine (**Supplementary Figs. 3e,f**). The oligomeric states of different mutants—S9A, S12A, S16A, H27A and Q30A—were verified by cross-linking. SDS-PAGE showed no substantial changes upon mutations in these pore-lining residues (**Supplementary Fig. 6**).

We found that the BM2$_{1-33}$ proton conductance (~14 H^{+} per s per channel) is about two-fold higher than that of AM2$_{18-60}$ (**Table 2**), consistent with results obtained from whole cell channel recording[6]. Conductance in all BM2 mutants was lower than in the WT (**Fig. 2b,c**). In particular, mutations S12A and S16A, in the middle of the pore between Ser9 and His19, had the largest effect, decreasing conductance by 45% and 44%, respectively. Replacing polar residues near the N- and C-terminal ends of the channel had less effect. The conductances of S9A, H27A and Q30A were lower than those of the WT by an average of ~27%. The above results suggest that not one but a combination of polar residues determines the proton conductance of BM2.

The cytoplasmic domain interacts with the matrix protein

The BM2 cytoplasmic domain has a noteworthy feature: the surface of the N-terminal half of the domain (residues 44–71) is almost entirely positive, whereas the surface of the C-terminal half (residues 72–103) is almost entirely negative (**Fig. 3a**). The charge separation results in a large electrostatic dipole moment, 4,215 Debye, at neutral pH; this dipole moment is about 4 s.d. above the mean for all proteins in PDB[21]. Moreover, the surface charges are highly conserved among different influenza B strains (**Supplementary Fig. 5b**). Reverse-genetics studies suggest that the cytoplasmic domain is involved in the incorporation of ribonucleoprotein (RNP) complex into viral particles, possibly through interaction with the M1 matrix proteins[16]. Indeed, the homology model of the N-terminal domain of BM1, derived from the crystal structure of AM1 (ref. 22) on the basis of 30% sequence identity (**Supplementary Fig. 7**), also shows a strong bipolar charge distribution (**Fig. 3b**). To investigate this interaction,

we made a water-soluble construct of BM2 that encompassed residues 43–109 but lacked the membrane-anchor residues. BM2$_{43-109}$ was used here instead of BM2$_{26-109}$ to avoid complications associated with the detergent required for solubilizing BM2$_{26-109}$. Equilibrium sedimentation experiments showed that BM2$_{43-109}$ forms a tetramer in water (**Supplementary Fig. 8**). The BM1 protein used in this experiment was fused at the N terminus to the maltose-binding protein (MBP), which prevented the substantial aggregation observed for BM1 protein that had been cleaved from the MBP tag.

We performed chemical shift perturbation of 2D ^{1}H-^{15}N correlation spectra of BM2$_{43-109}$ by MBP-BM1. At 1:1 molar ratio of BM2$_{43-109}$ to MBP-BM1, the majority of resonances of BM2$_{43-109}$ are broadened and a specific set of resonances shifted substantially (**Fig. 3c**), whereas the spectrum is not perturbed by MBP alone (see negative control in **Supplementary Fig. 9**). The perturbed resonances that could be correctly assigned are mostly from the last amphipathic helix of BM2, on which the solvent-exposed surface is negatively charged (**Fig. 3d**). Therefore, the interaction between BM2 and BM1 is electrostatically driven, possibly between the negatively charged C-terminal end of BM2 (residues 84–108) and the positively charged surface of the N-terminal domain of BM1.

DISCUSSION

Although the overall assembly of TM helices of BM2 is similar to that of AM2—for example, both are left-handed four-helix bundles with

Table 2 Proton conductance rates[a]

	Conductance per tetramer	No. samples	s.d.	% of BM2 WT
BM2 WT	14.7	4	1.3	100%
S9A	10.5	3	0.4	71%
S12A	8.2	4	1.5	55%
S16A	8.3	5	1.3	56%
H27A	10.8	4	3.7	74%
Q30A	12.7	3	1.4	75%
AM2 WT	7.0	2	0.3	47%
Lipids	0.08	4	0.3	

[a]Proton conduction rates were measured as the initial rate of change upon dropping the external pH to 6.05–6.10 (internal pH 7.7). Rates are given in protons per s per channel.
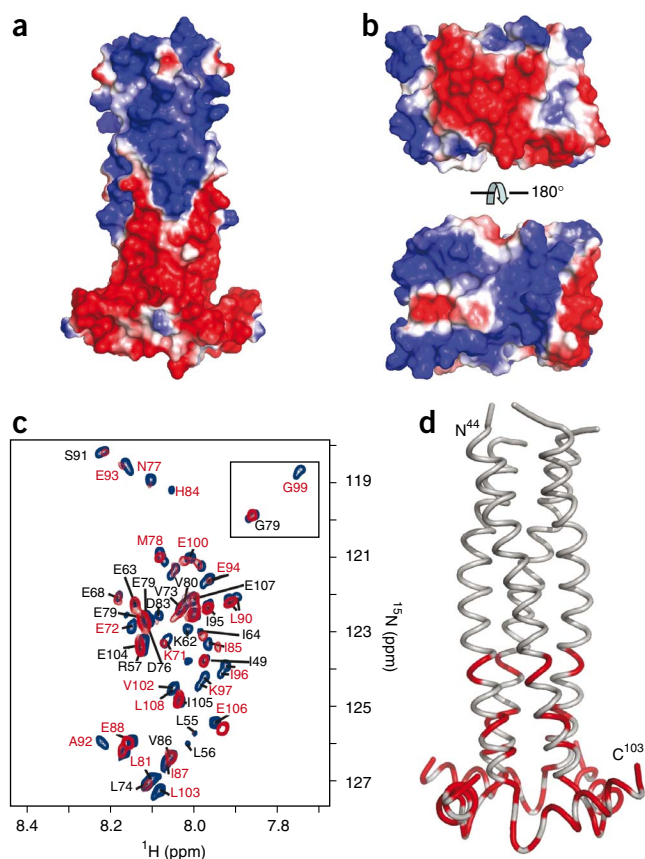
Figure 3 Interaction between BM2 cytoplasmic domain and BM1 matrix protein. (**a**) Surface charge representation of the BM2 cytoplasmic domain, showing the strong segregation of positive (blue) and negative (red) charges. (**b**) Surface charge representation of the N-terminal domain of BM1 (residues 1–156). The homology model of $BM1_{1-156}$ was built on the basis of the crystal structure of $AM1_{1-158}$ (ref. 22) and the 30% sequence identity between the two proteins (**Supplementary Fig. 7**). (**c**) Overlay of ^1H-^{15}N TROSY spectra of $BM2_{43-109}$ in the absence (blue) and presence (red) of MBP-BM1. The labeled resonances are those whose assignments could be correctly traced. (**d**) Mapping of perturbed resonances onto the cytoplasmic domain structure. The perturbed regions are colored in red.

a hydrophilic pore—the two channels' assemblies differ substantially in details. Unlike AM2, the TM domain of BM2 shows strong coiled-coil characteristics with heptad repeats. It is the first of its kind in the known ion channel structures that adopts a coiled-coil assembly to conduct ions. The coiled-coil arrangement allows the TM segment of BM2 to form a stable tetramer by itself, but stable channel assembly of AM2 also requires a C-terminal amphipathic helix following the TM domain[10]. Indeed, the BM2 TM domain (residues 1–33) runs as a tetramer in SDS-PAGE (**Supplementary Fig. 10**), but the same did not occur with the AM2 TM domain (residues 20–46) (ref. 10). Another important difference is that the rimantadine binding observed in the AM2 structure is absent in BM2, which may explain the drug resistance of the BM2 channel. The drug's binding site is the lipid-facing pocket observed in the NMR structure of the AM2 channel, which consists of Trp41, Ile42 and Arg45 from one TM helix and Leu40, Leu43 and Asp44 from the adjacent TM helix. The corresponding residues in BM2 are Trp23, Thr24 His27 from one TM helix and Ala22, Ile26 and Gly26 from the adjacent TM helix. The above two groups of residues are uncorrelated and thus do not constitute surfaces of similar electrostatic and hydrophobic properties (**Supplementary Fig. 11**).

The BM2 channel structure suggests a number of polar residues important for both hydration of the channel pore and support for proton passage during channel activation. Mutating the serines on the N-terminal side of the Trp23 gate to alanine substantially reduced proton conductance, with the largest decrease (~45%) observed for S12A and S16A. Serines 9, 12 and 16 are pore lining and important for pore hydration. The Ser12 side chain is completely facing the pore and, unlike those of Ser9 and Ser16, is not involved in helical packing; it is conveniently positioned for relaying protons. It was shown previously that mutating the pH sensor, His19, to alanine markedly
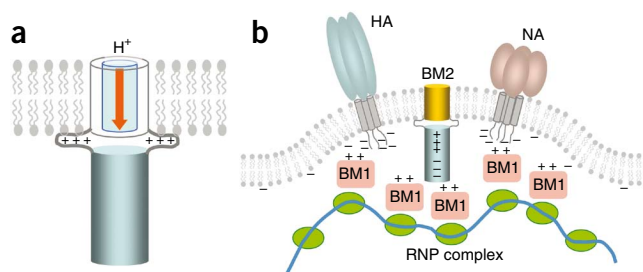
decreases conductance[23]. Together, these results suggest that the serines are involved in relaying hydronium ions or coordinating water molecules that may form a proton wire to relay protons to His19. Protonating the histidines then leads to opening of the Trp23 gate by a mechanism that is still not understood. Compared to the channel pore of AM2, which is also very hydrophilic[24], the BM2 pore has two more serine hydroxyl groups that can facilitate proton relay. This difference may in part explain the higher conductance of the BM2 channel. Mutating residues on the C-terminal side of the Trp23 gate, H27A and Q30A, also reduced conductance by ~25%. His27 and Asn30 are exposed to the hydrophilic region of the membrane; they probably facilitate proton exit. It is interesting to note that after the tryptophan gate opens, polar residues are also present in AM2 (Asp44 and Arg45), and replacing Asp44 with alanine results in a three-fold decrease in conductance[18].

Perturbation of the chemical environment of a defined region of the cytoplasmic domain by the M1 matrix protein indicates specific molecular recognition between the two proteins. The perturbed region identified, from residues 84 to 108, is consistent with known deletions and mutations of BM2 that affect virus assembly. For viruses in which residues 101–109 are deleted from BM2, the RNP complex is greatly reduced in size and membrane association of M1 is altered[16]. Furthermore, alanine-scanning substitution of three consecutive residues showed that the 86–88A, 89–91A, 93–94A and 95–97A mutants do not grow normally and contain substantially reduced levels of M1 and nucleoprotein[16]. Data from structural and reverse-genetics studies indicate that the interaction between the cytoplasmic regions of the proton channels and matrix proteins are important in viral assembly. During virus budding, the matrix proteins and RNPs must coat the plasma membrane such that budding will result in a properly assembled virus. Therefore, the membrane patch that is destined to bud out from the host cell must contain specific sites for recruiting the matrix protein and RNP complexes (**Fig. 4**). The unusually strong electric dipole moment of BM2 cytoplasmic domain may serve to

Figure 4 The dual functionality of BM2. The channel domain serves to conduct proton across the viral and trans-Golgi membrane (left). The cytoplasmic domain is involved in recruiting the M1 matrix proteins and RNP complexes to the budding membrane (right).

orient the M1 matrix protein, which also has a strong electric dipole moment, for specific association. Electric dipole–facilitated molecular recognition is commonly observed in cellular signaling pathways: for example, in the interactions between the caspase recruitment domains[25]. The coating of M1 and RNPs to the virus membrane is likely achieved through cooperative interactions between M1 and the negatively charged membrane, the short cytoplasmic tails of hemagglutinin and neuraminidase, and the cytoplasmic domain of M2.

METHODS

Methods and any associated references are available in the online version of the paper at http://www.nature.com/nsmb/.

Accession codes. Protein Data Bank: Coordinates for the channel domain and cytoplasmic domain have been deposited with accession codes 2KIX and 2KJ1, respectively.

Note: Supplementary information is available on the Nature Structural & Molecular Biology website.

1. Hatta, M., Goto, H. & Kawaoka, Y. Influenza B virus requires BM2 protein for replication. *J. Virol.* **78**, 5576–5583 (2004).
2. Pinto, L.H. & Lamb, R.A. The M2 proton channels of influenza A and B viruses. *J. Biol. Chem.* **281**, 8997–9000 (2006).
3. Hay, A.J., Wolstenholme, A.J., Skehel, J.J. & Smith, M.H. The molecular basis of the specific anti-influenza action of amantadine. *EMBO J.* **4**, 3021–3024 (1985).
4. Helenius, A. Unpacking the incoming influenza virus. *Cell* **69**, 577–578 (1992).
5. Paterson, R.G., Takeda, M., Ohigashi, Y., Pinto, L.H. & Lamb, R.A. Influenza B virus BM2 protein is an oligomeric integral membrane protein expressed at the cell surface. *Virology* **306**, 7–17 (2003).
6. Mould, J.A. *et al.* Influenza B virus BM2 protein has ion channel activity that conducts protons across membranes. *Dev. Cell* **5**, 175–184 (2003).
7. Pinto, L.H. *et al.* A functionally defined model for the M2 proton channel of influenza A virus suggests a mechanism for its ion selectivity. *Proc. Natl. Acad. Sci. USA* **94**, 11301–11306 (1997).
8. Kovacs, F.A., Denny, J.K., Song, Z., Quine, J.R. & Cross, T.A. Helix tilt of the M2 transmembrane peptide from influenza A virus: an intrinsic property. *J. Mol. Biol.* **295**, 117–125 (2000).
9. Kukol, A., Adams, P.D., Rice, L.M., Brunger, A.T. & Arkin, T.I. Experimentally based orientational refinement of membrane protein models: A structure for the influenza A M2 H+ channel. *J. Mol. Biol.* **286**, 951–962 (1999).
10. Schnell, J.R. & Chou, J.J. Structure and mechanism of the M2 proton channel of influenza A virus. *Nature* **451**, 591–595 (2008).
11. Wang, J., Kim, S., Kovacs, F. & Cross, T.A. Structure of the transmembrane region of the M2 protein H+ channel. *Protein Sci.* **10**, 2241–2250 (2001).
12. Stouffer, A.L. *et al.* Structural basis for the function and inhibition of an influenza virus proton channel. *Nature* **451**, 596–599 (2008).
13. Ma, C. *et al.* Identification of the pore-lining residues of the BM2 ion channel protein of influenza B virus. *J. Biol. Chem.* **283**, 15921–15931 (2008).
14. Chen, B.J., Leser, G.P., Jackson, D. & Lamb, R.A. The influenza virus M2 protein cytoplasmic tail interacts with the M1 protein and influences virus assembly at the site of virus budding. *J. Virol.* **82**, 10059–10070 (2008).
15. McCown, M.F. & Pekosz, A. Distinct domains of the influenza a virus M2 protein cytoplasmic tail mediate binding to the M1 protein and facilitate infectious virus production. *J. Virol.* **80**, 8178–8189 (2006).
16. Imai, M., Kawasaki, K. & Odagiri, T. Cytoplasmic domain of influenza B virus BM2 protein plays critical roles in production of infectious virus. *J. Virol.* **82**, 728–739 (2008).
17. Imai, M., Watanabe, S., Ninomiya, A., Obuchi, M. & Odagiri, T. Influenza B virus BM2 protein is a crucial component for incorporation of viral ribonucleoprotein complex into virions during virus assembly. *J. Virol.* **78**, 11007–11015 (2004).
18. Pielak, R.M., Schnell, J.R. & Chou, J.J. Mechanism of drug inhibition and drug resistance of influenza A M2 channel. *Proc. Natl. Acad. Sci. USA* **106**, 7379–7384 (2009).
19. Xu, C. *et al.* Regulation of T cell receptor activation by dynamic membrane binding of the CD3epsilon cytoplasmic tyrosine-based motif. *Cell* **135**, 702–713 (2008).
20. Harbury, P.B., Zhang, T., Kim, P.S. & Alber, T. A switch between two-, three-, and four-stranded coiled coils in GCN4 leucine zipper mutants. *Science* **262**, 1401–1407 (1993).
21. Felder, C., Prilusky, J., Silman, I. & Sussman, J. A server and database for dipole moments of proteins. *Nucleic Acids Res.* **35** (special Web Servers Issue) (2007).
22. Sha, B. & Luo, M. Structure of a bifunctional membrane-RNA binding protein, influenza virus matrix protein M1. *Nat. Struct. Biol.* **4**, 239–244 (1997).
23. Otomo, K., Toyama, A., Miura, T. & Takeuchi, H. Interactions between histidine and tryptophan residues in the BM2 proton channel from influenza B virus. *J. Biochem.* **145**, 543–554 (2009).
24. Du, Q.S., Huang, R.B., Wang, C.H., Li, X.M. & Chou, K.C. Energetic analysis of the two controversial drug binding sites of the M2 proton channel in influenza A virus. *J. Theor. Biol.* **259**, 159–164 (2009).
25. Chou, J.J., Matsuo, H., Duan, H. & Wagner, G. Solution structure of the RAIDD CARD and model for CARD/CARD interaction in caspase-2 and caspase-9 recruitment. *Cell* **94**, 171–180 (1998).
26. Smart, O.S., Goodfellow, J.M. & Wallace, B.A. The pore dimensions of gramicidin A. *Biophys. J.* **65**, 2455–2460 (1993).

ONLINE METHODS

Sample preparation. BM2 gene from influenza B (the Maryland/01 strain) with the C11S mutation was *E. coli* codon–optimized and synthesized (Epoch Biolabs). The BM2$_{1-33}$ construct was cloned into the pMALc2x vector (New England Biolabs) and expressed as MBP fusion protein. MBP-BM2$_{1-33}$ was purified from cell lysis using amylose resin. The fusion protein was cleaved with TEV protease, and BM2$_{1-33}$ was isolated by reverse-phase HPLC. BM2$_{1-33}$ was dissolved in a solution containing 8 M urea and DHPC and then dialyzed to remove the denaturant. After concentration, the sample typically contained 0.7 mM BM2$_{1-33}$, ~300 mM DHPC, 15 mM β-mercaptoethanol and 40 mM sodium phosphate (pH 7.5). BM2$_{26-109}$ was expressed with C-terminal 6His tag using the pET21a vector. The overexpressed protein formed an inclusion body, which was dissolved in 6 M guanidine HCl and then purified using nickel resin. After dialysis to remove denaturant, the precipitated BM2$_{26-109}$ was reconstituted in LMPG detergent using a dialysis procedure similar to that used for BM2$_{1-33}$ above. A typical NMR sample contained 0.7 mM protein, 200 mM LMPG, 15 mM β-mercaptoethanol, 25 mM NaCl and 25 mM Tris-HCl (pH 6.8).

Liposomal H$^+$ flux assay. The liposomal H$^+$ flux assay was established on the basis of earlier work[18]. BM2$_{1-33}$ channels were reconstituted into liposomes by mixing 10 mg of *E. coli* polar lipid extract, 5 nmol of BM2$_{1-33}$ peptide and 0.2 nmol of valinomycin in chloroform-methanol mixture. A thin film was formed and then resuspended in a strong buffer (50 mM phosphate, 50 mM citrate, 122 mM KCl, 122 mM NaCl, 0.01% (w/v) NaN$_3$, pH 7.7) and extruded through 0.2-μM polycarbonate membranes. The external buffer was exchanged with a weak buffer (2 mM phosphate, 2 mM citrate, 122 mM KCl, 122 mM NaCl, 0.01% (w/v) NaN$_3$, pH 7.8). Final eluted volume was 1.5 ml, containing 5 mg ml^{-1} lipid, 3 μM peptide and 0.1 μM valinomycin. Proton conductance was initiated by addition of 3.5 μl of 1 M HCl with rapid mixing and terminated by the addition of 5 μM of carbonyl cyanide *m*-chlorophenylhydrazone (FCCP), which equilibrated pH on both sides of the membrane. Proton flux was monitored by measurement of external pH.

BM2-BM1 interaction. BM2$_{43-109}$ was cloned with N-terminal 6His-tag into the pET21a vector. Protein was expressed in inclusion body and purified using a procedure similar to that for BM2$_{26-109}$. The BM1 gene from the same virus strain was cloned into the pMALc2x vector and expressed as MBP fusion protein. MBP-BM1 was purified with amylose resin followed by Mono-Q ion exchange purification. To obtain MBP protein as a negative control for the BM2-BM1 interaction experiment, MBP-BM1 was cleaved with TEV protease. The released MBP was purified by Mono-Q. The purified BM2$_{43-109}$, MBP-BM1 and MBP were dialyzed against a NMR buffer consisting of 25 mM Tris-HCl (pH 6.8), 25 mM NaCl and 15 mM β-mercaptoethanol. To investigate specific interaction between BM2 and BM1, 0.3 mM (monomer concentration) of BM2$_{43-109}$ was mixed with 0.3 mM of MBP-BM1 or MBP. 2D ^{1}H-^{15}N TROSY spectra of the mixed samples were recorded on a Bruker 750 MHz spectrometer.

NMR spectroscopy. NMR experiments were conducted at 30 °C on spectrometers equipped with cryogenic probes (Bruker). Sequence specific assignment of backbone and side chain resonances are described in **Supplementary Methods** and shown in **Supplementary Figures 10** and **12**.

For BM2$_{1-33}$, intrasubunit NOEs involving both backbone and side chain protons were assigned using the 3D ^{15}N-edited and ^{13}C-edited NOESYs recorded with NOE mixing times of 110 and 150 ms, respectively, on a sample containing ^{15}N- and ^{13}C-labeled protein and deuterated DHPC (D35-DHPC) (Avanti Polar Lipids). To identify contacts between neighboring subunits, intrasubunit NOEs were first assigned to completion. This was possible given the low complexity of the NOESY spectra (for example, see **Supplementary Fig. 13**). The remaining NOEs, which could not be explained by intrasubunit distances on the basis of the known secondary structures, were identified as intersubunit NOEs. For BM2$_{26-109}$, the NOESY spectra were collected with deuterated LMPG (D27-LMPG). A similar approach to NOE assignment was used for BM2$_{1-33}$, except for additional 3D NOESY spectra of ILV-labeled protein that were recorded to resolve the increased spectral complexity.

The χ$_1$ rotamers were obtained from measurements of the three-bond scalar couplings including $^3J_{NC\gamma}$ and $^3J_{C'C\gamma}$[27]. Backbone ^{1}H-^{15}N residual dipolar couplings (RDCs) were measured for the complex of BM2$_{26-109}$ and LMPG micelle in the G-Tetrad DNA alignment medium[28].

Structure determination. Structures were calculated using the program XPLOR-NIH[29]. The secondary structure of the monomer was first calculated from random coil using intrasubunit NOEs, backbone dihedral restraints derived from chemical shifts (TALOS)[30] and side chain χ$_1$ restraints. A total of 20 monomer structures were calculated using a high-temperature simulated annealing (SA) protocol in which the bath temperature was cooled from 1,000 to 200 K. To obtain an initial set of tetramer structures, four copies of the lowest-energy monomer structure calculated above were used. The same SA run was performed in the presence of intersubunit NOEs and all other intrasubunit restraints. For each experimental intersubunit NOE between two adjacent subunits, four identical distance restraints were assigned to all respective pairs of neighboring subunits to satisfy the condition of C4 rotational symmetry. During the annealing run, the bath was cooled from 1,000 to 200 K. A total of 100 tetramer structures were calculated. For BM2$_{1-33}$, 15 low-energy structures were selected as the structural ensemble. Ramachandran plot statistics are as follows: most favored (90.7%), additionally allowed (7.4%), generously allowed (1.9%) and disallowed (0%).

For BM2$_{26-103}$, for which RDCs are available, 15 structures whose individual subunits have on average the best agreement with RDCs (r ~0.65 and Q ~0.52) were selected for low-temperature refinement (bath-cooled from 200 to 20 K) against RDCs in the presence of all other restraints. For each of those 15 structures, 10 RDC-refined structures were generated. From that set, the structure with the lowest total energy was added to the final ensemble to describe the structural diversity of the solution structure. Without violating any NOE restraints, the final subunit structures fit RDCs to r of 0.88 and Q of 0.12, with D_a = 9.0 Hz and R_h = 0.62. Ramachandran plot statistics are as follows: most favored (83.3%), additionally allowed (15.3%), generously allowed (1.4%) and disallowed (0%).

27. Bax, A. *et al.* Measurement of homo- and heteronuclear J couplings from quantitative J correlation. *Methods Enzymol.* **239**, 79–105 (1994).
28. Lorieau, J., Yao, L. & Bax, A. Liquid crystalline phase of G-tetrad DNA for NMR study of detergent-solubilized proteins. *J. Am. Chem. Soc.* **130**, 7536–7537 (2008).
29. Schwieters, C.D., Kuszewski, J., Tjandra, N. & Clore, G.M. The Xplor-NIH NMR molecular structure determination package. *J. Magn. Reson.* **160**, 66–74 (2002).
30. Cornilescu, G., Delaglio, F. & Bax, A. Protein backbone angle restraints from searching a database for chemical shift and sequence homology. *J. Biomol. NMR* **13**, 289–302 (1999).